Structural insight into the recognition of pathogen-derived phosphoglycolipids by C-type lectin receptor DCAR

Received for publication, January 22, 2020, and in revised form, March 2, 2020 Published, Papers in Press, March 5, 2020, DOI 10.1074/jbc.RA120.012491

Zakaria Omahdi,[a,b,c] Yuto Horikawa,[d] Masamichi Nagae,[a,b,e] Kenji Toyonaga,[a,b] Akihiro Imamura,[f,g] Koichi Takato,[f] Takamasa Teramoto,[h] Hideharu Ishida,[f,g,i] Yoshimitsu Kakuta,[d,h,1] and Sho Yamasaki[a,b,c,j,k,2]

From the [a]Department of Molecular Immunology, Research Institute for Microbial Diseases and the [b]Laboratory of Molecular Immunology, Immunology Frontier Research Center (IFReC), Osaka University, Suita 565-0871, Japan, the [c]Division of Molecular Immunology, Medical Institute of Bioregulation, Kyushu University, Fukuoka 812-8582, Japan, the [d]Laboratory of Structural Biology, Graduate School of System Life Sciences and the [h]Department of Bioscience and Biotechnology, Faculty of Agriculture, Kyushu University, 744 Moto-oka, Nishi-ku, Fukuoka 819-0395, Japan, the [e]Department of Pharmaceutical Sciences, University of Tokyo, Bunkyo-Ku, Tokyo 113-0033, Japan, the [f]Department of Applied Bioorganic Chemistry, Faculty of Applied Biological Sciences, the [g]United Graduate School of Agricultural Science, and the [i]Center for Highly Advanced Integration of Nano and Life Sciences, Gifu University, Gifu 501-1193, Japan, [j]Division of Molecular Design, Medical Institute of Bioregulation, Kyushu University, Fukuoka 812-8582, Japan, and the [k]Division of Molecular Immunology, Medical Mycology Research Center, Chiba University, Chiba 260-8673, Japan

Edited by Gerald W. Hart

The C-type lectin receptors (CLRs) form a family of pattern recognition receptors that recognize numerous pathogens, such as bacteria and fungi, and trigger innate immune responses. The extracellular carbohydrate-recognition domain (CRD) of CLRs forms a globular structure that can coordinate a Ca^{2+} ion, allowing receptor interactions with sugar-containing ligands. Although well-conserved, the CRD fold can also display differences that directly affect the specificity of the receptors for their ligands. Here, we report crystal structures at 1.8–2.3 Å resolutions of the CRD of murine dendritic cell-immunoactivating receptor (DCAR, or *Clec4b1*), the CLR that binds phosphoglycolipids such as acylated phosphatidyl-*myo*-inositol mannosides (AcPIMs) of mycobacteria. Using mutagenesis analysis, we identified critical residues, Ala^{136} and Gln^{198}, on the surface surrounding the ligand-binding site of DCAR, as well as an atypical Ca^{2+}-binding motif (Glu-Pro-Ser/$EPS_{168-170}$). By chemically synthesizing a water-soluble ligand analog, inositol-monophosphate dimannose (IPM2), we confirmed the direct interaction of DCAR with the polar moiety of AcPIMs by biolayer interferometry and co-crystallization approaches. We also observed a hydrophobic groove extending from the ligand-binding site that is in a suitable position to interact with the lipid portion of whole AcPIMs. These results suggest that the hydroxyl group-binding ability and hydrophobic groove of DCAR mediate its specific binding to pathogen-derived phosphoglycolipids such as mycobacterial AcPIMs.

The recognition of pathogens by the innate immune system is one of the initial steps leading to a robust and well-orchestrated immune response (1). This physiological process is in part made possible by the presence of proteins at the surface of the immune cell called pattern-recognition receptors. Among these, C-type lectin receptors (CLRs)[3] form a family of pattern recognition receptors that were shown to recognize not only a broad spectrum of pathogens, but also endogenous molecules released by stressed or dying cells, through their interaction with ligands of various types and structures (2–4). Most of these receptors share the same domain organization: they are type II transmembrane proteins with a cytoplasmic intracellular tail, a transmembrane domain, and an extracellular domain composed of both the stalk region as well as the compact and globular carbohydrate-recognition domain (CRD) (5). Through its ability to coordinate Ca^{2+} ions, the CRD is, for most CLRs, of paramount importance to bind sugar-containing ligands.

Dendritic cell immunoactivating receptor (DCAR, or *Clec4b1*) is a CLR expressed by myeloid cells that was originally described by high sequence similarity with dendritic cell immunoreceptor 1 (DCIR1, or *Clec4a2*) in mouse (6). Although they share 91% similarity in their CRDs, differences were observed in their stalk and intracellular domains. Contrarily to DCIR1, which has an immunoreceptor tyrosine-based inhibitory motif (ITIM) within its own intracellular domain, the adaptor mole-

This work was supported by the Japan Agency for Medical Research and Development Grants JP19gm0910010, JP19ak0101070, and JP19fk0108075; by Japan Society for the Promotion of Science KAKENHI Grant 17H04087; and by funds from the Takeda Science Foundation. The authors declare that they have no conflicts of interest with the contents of this article.

This article contains Table S1 and Figs. S1–S8.

The atomic coordinates and structure factors (codes 6LKR, 6KZR, and 6LFJ) have been deposited in the Protein Data Bank (http://wwpdb.org/).

[1] To whom correspondence may be addressed: Dept. of Bioscience and Biotechnology, Faculty of Agriculture, Kyushu University, Fukuoka 819-0395, Japan. E-mail: kakuta@agr.kyushu-u.ac.jp.

[2] To whom correspondence may be addressed: Dept. of Molecular Immunology, Research Institute for Microbial Diseases, Osaka University, Suita 565-0871, Japan. Tel.: 81-6-6879-8306; Fax: 81-6-6879-8308; E-mail: yamasaki@biken.osaka-u.ac.jp.

[3] The abbreviations used are: CLR, C-type lectin receptor; CRD, carbohydrate-recognition domain; DCAR, dendritic cell-immunoactivating receptor; DCIR, dendritic cell immunoreceptor; PDB, Protein Data Bank; AcPIM, acylated phosphatidyl-*myo*-inositol mannoside; FcRγ, Fc receptor γ chain; ITAM, immunoreceptor tyrosine-based activation motif; BDCA, blood dendritic cell antigen; h, human; m, mouse; BLI, biolayer interferometry; DC-SIGN, dendritic cell–specific ICAM-3 grabbing nonintegrin; IPM2, inositol-monophosphate dimannose.

cule Fc receptor γ chain (FcRγ) harboring an immunoreceptor tyrosine-based activation motif (ITAM) is required for DCAR-dependent signaling (6, 7).

We recently reported that DCAR functions as a receptor for mycobacteria through the recognition of unique phosphoglycolipids abundantly found in mycobacterial envelopes, called acylated phosphatidyl-*myo*-inositol mannosides (AcPIMs) (8). This induces MCP-1 production from monocyte-derived inflammatory cells and promotes a Th1-mediated protective response, thereby contributing to the immune response against mycobacteria in mouse (7). However, the molecular and structural basis of phosphate-containing glycolipid recognition by DCAR remains to be clarified. Human DCIR and blood dendritic cell antigen 2 (BDCA-2) are closely related to DCAR, but its own human ortholog has yet to be identified (9, 10). However, AcPIMs induce similar sets of inflammatory genes in human dendritic cells (7), implying that humans express unidentified AcPIM receptor, and thus the determination of murine DCAR structure may provide valuable information for the identification of novel bacterial receptor(s).

The present study shows that DCAR has an overall typical C-type lectin fold that allows it to bind carbohydrates in similar fashion to other CLRs. Structural and mutagenesis analysis also revealed its characteristics for the suitable recognition of unique mycobacterial phosphoglycolipids.

Results

DCAR preparation, crystallization, and structural determination

The CRD (residues 78–209) of murine DCAR was expressed as inclusion bodies in *Escherichia coli* and then refolded *in vitro* by a dilution method. Refolding of DCAR did not require Ca^{2+} ions, and refolded proteins were purified by anion exchange followed by gel-filtration chromatography (Fig. S1, *A* and *B*). The elution profile of the refolded CRD displayed a single homogenous and sharp peak at the expected molecular weight, indicating that conformational variations were unlikely and that the CRD behaves as a monomer after refolding (Fig. S1*A*). DCAR CRD crystals were obtained by the sitting-drop method, the structure was solved at a resolution of 2.3 Å, and the asymmetric unit contained two DCAR molecules (Table 1). The structure of DCAR is composed of two flanking antiparallel α-helices (α1 and α2) and nine β-strands (β1 to β9) and is stabilized by three disulfide bonds similar to other CLR family members (Fig. 1). These results thus show that DCAR has an overall typical C-type lectin domain fold.

Structural comparison of DCAR and Mincle

The CRD of the similar CLR Mincle (Fig. 2*B*), which has been determined as the disaccharide trehalose complex, has 43% sequence similarity with the CRD of DCAR (Fig. 2*A*) and was used for structural comparison (11). Superimposition of DCAR and cow Mincle (Fig. 2*B*; PDB code 4ZRW) shows that the position of backbone Cα atoms in both CRDs are similar, with a root-mean-square deviation of 0.627 Å for 129 structurally equivalent Cα atoms (Fig. 2*C*). Although Mincle binds three ions, whereas DCAR binds only one, the position of the Ca^{2+} ion of the primary sugar-binding site is also nearly the same between the two proteins (Fig. 2, *A*–*C*). The canonical EPN (Glu-Pro-Asn) motif of the primary sugar-binding site of Mincle (residues 168–170) is typically found in glucose/mannose binding CLRs, as opposed to the QPD (Gln-Pro-Asp) motif, which generally indicates a preference toward galactose-containing ligands (5, 12). DCAR bears a similar but unusual EPS (Glu-Pro-Ser) sequence (residues 168–170), also found in several members of the DCIR family (13). As shown by the crystal structure of hDCIR (PDB code 5B1X), the EPS sequence can successfully coordinate a Ca^{2+} ion and contribute to mannose recognition (13). In line with this report, DCAR also bound a Ca^{2+} ion through its EPS sequence, as well as two additional residues of the WND motif (residues 189–191) which is well-conserved among CLRs (Figs. 1, *green filled circles*, and 2*D*). Despite this sequence difference, the Ca^{2+}-binding site location and the position of the amino acids of DCAR and Mincle are nearly identical (Fig. 2, *D*–*F*), with the exception of the residues following the EPN motif in Mincle that interact with another Ca^{2+} ion and are protruding compared with the corresponding amino acids of DCAR (Fig. 2*C*). The overall structural comparison therefore confirms that the CRD of DCAR has a typical C-type lectin domain fold and can coordinate a Ca^{2+} ion through its EPS sequence.

Table 1
Data collection and refinement statistics.

	Ligand-free	Glycerol complex	IPM2 complex
Data collection			
Space group	$P2_12_12_1$	$P2_12_12_1$	$P2_12_12_1$
Unit cell parameters (Å)			
a	64.4	66.0	65.7
b	72.1	72.4	72.6
c	100.6	101.1	100.5
Wavelength (Å)	1.0000	1.0000	1.0000
Resolution range (Å)	50.0–1.85	58.9–2.30	48.8–1.84
No. of reflections			
Observed	268,974	158,838	280,261
Unique	77,390	22,007	80,659
Redundancy	3.5 (3.5)	7.2 (7.2)	3.5 (3.3)
R_{sym} (overall/outer shell)	0.064 (0.817)	0.120 (0.687)	0.143 (0.800)
$I/\sigma(I)$	10.9 (1.27)	15.1 (3.00)	5.60 (1.00)
$CC_{½}$ (%)	99.8 (51.9)		
Completeness (%)	99.3 (98.5)	99.7 (98.6)	99.6 (99.4)
Refinement statistics			
Resolution range (Å)	48.1–1.84	44.0–2.30	48.8–1.84
No. of reflections			
Working set	38,931	20,861	40,178
Test set	1999	1141	1981
Completeness (%)	99.74	99.72	99.45
R_{cryst} (%)/R_{free} (%)	18.2/20.5	14.7/21.2	16.04/20.4
Root mean square deviation			
Bond length (Å)	0.013	0.013	0.013
Bond angles (°)	1.634	1.629	1.674
Average B-factor (Å²)/no. of atoms			
Protein	37.19/2331	35.52/2261	31.31/2312
Ca^{2+}	36.99/2	23.98/2	34.66/2
Water	46.03/235	47.05/243	43.25/290
Glycerol		43.23/24	
IPM2			71.39/65
Bis–Tris–propane	58.58/19		59.28/19
Ramachandran analysis			
Favored (%)	89.70	90.91	91.18
Allowed (%)	8.15	7.44	5.88
Outlier (%)	2.15	1.65	2.94

The EPS motif of DCAR is required for optimal function

As mentioned above, DCAR coordinates its Ca^{2+} ion through an EPS sequence, which was shown to mediate man-

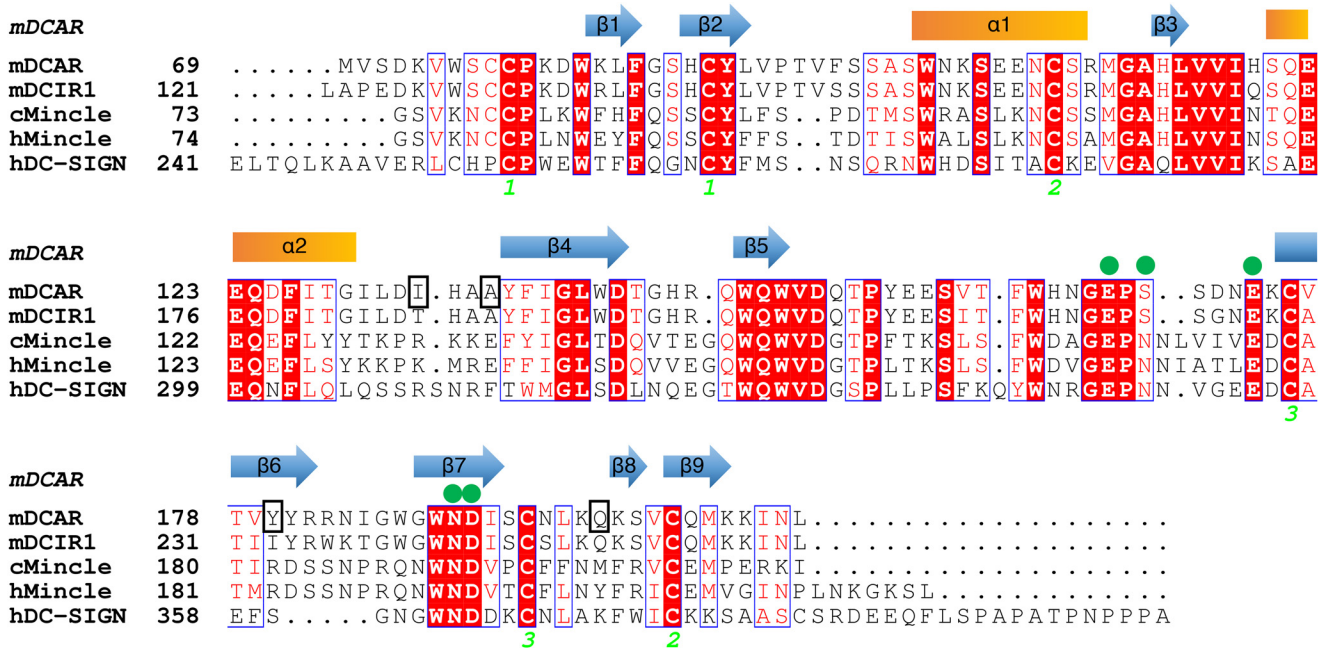

Figure 1. Structure based sequence alignment of DCAR, Mincle, DCIR1, and DC-SIGN. Amino acid sequence alignment of the extracellular domains of DCAR, Mincle, DCIR1, and DC-SIGN (dendritic cell-specific ICAM-3 grabbing nonintegrin), with identical residues highlighted in *red* and similar residues enclosed in *blue boxes* (*m*, mouse; *c*, cow; *h*, human). Secondary structure elements (α-helices and β-strands) of DCAR are shown above the primary structures, and each pair of cysteines involved in disulfide-bond formation are designated by a *number* below the sequences. The *green filled circles* indicate the residues participating in Ca^{2+} coordination, and the residues involved in ligand binding are enclosed in *black boxes*. Sequence alignment was obtained with ESPript (33).

nose binding by hDCIR (13). This sequence is also found in two other members of the DCIR family. We thus sought to test whether this unusual EPS sequence is necessary for ligand binding by DCAR. For comparison, we generated a DCAR–Ig fusion protein, composed of the Fc portion of human IgG fused to the extracellular domain of DCAR (stalk and CRD), which bears the well-established EPN motif instead of the EPS sequence ($DCAR^{EPN}$–Ig). Binding of $DCAR^{EPN}$–Ig to plate-coated AcPIM2 was significantly reduced when compared with DCAR–Ig (Fig. S2*A*). An even stronger decrease in signaling activity was observed when stimulating reporter cells expressing the $DCAR^{EPN}$ mutant with AcPIMs (Fig. S2*B*). These results thus indicate that the EPS sequence is indeed a Ca^{2+}-binding motif and necessary for optimal ligand binding and signaling through DCAR. Furthermore, an additional electron density corresponding to a glycerol molecule is observed adjacent the Ca^{2+} coordination site (Fig. 3*A*, *left panel*), and the comparison with the location of trehalose in the structure of Mincle (PDB code 4KZV) showed that the two OH groups of glycerol were in a similar position to that of the 3- and 4-OH groups of trehalose (Fig. 3*B*) (14). Furthermore, we also observed two H_2O molecules in the same position in the ligand-free DCAR crystals grown in a glycerol-free condition (Fig. S3*A*). These results suggest that DCAR, through its atypical EPS motif, interacts with the sugar moiety of its ligands.

Ligand recognition requires the short and neutral residue Ala^{136}

Unlike the conserved residues of the Ca^{2+} coordination site, the ones surrounding it are rather different between DCAR and Mincle (Fig. 3*B*). Among these, we first assessed the role of the Ala^{136} (Glu^{135} in Mincle) by mutagenesis. Because DCAR ligands bear a negatively charged phosphate (7), we surmised that, contrarily to Mincle, the non-negative and relatively short side chain of Ala^{136} was required to accommodate a phosphate moiety in this area. We therefore introduced a negatively charged Glu (the corresponding residue of Mincle; $DCAR^{A136E}$) or Asp ($DCAR^{A136D}$) at this position and induced the expression of the mutant receptors in reporter cells. The presence of a negatively charged residue at this position as is the case for Mincle, abolished GFP expression in response to ligand stimulation (Fig. 3*C*), implying that a negative charge in the vicinity of the primary sugar-binding site may prevent the interaction with AcPIMs. To examine the impact of the size of the side chain, we substituted the neutral Ala^{136} with neutral residues of increasing side-chain length (Val < Leu/Ile). Although the mutant with the shortest residue ($DCAR^{A136V}$) retained significant reporter activity, the $DCAR^{A136L}$ and $DCAR^{A136I}$ mutants showed strongly reduced activation (Fig. 3*D*). These results were confirmed by the introduction of these mutations in DCAR–Ig fusion proteins, which had a similar effect on direct binding to plate-coated AcPIMs (Fig. 3*E* and Fig. S2*C*). It thus suggests that the Ala^{136} is required to avoid electrostatic and steric hindrance with the phosphate moiety of AcPIMs.

Critical role of Gln^{198} for ligand binding

The residues corresponding to the Gln^{198} of DCAR (Fig. 3*B*) in mDCIR2, hDCIR, and hDectin-2 (His^{225}, Gln^{226}, and Arg^{198}, respectively) were shown to be part of a secondary sugar-binding site in these three closely related CLRs (13, 15, 16). Consistent with these results, Gln^{198} was shown to be required for DCAR, because substitution with Ala and the slightly shorter Asn both abolished binding efficiency (Fig. S2*D*). Moreover, the strong reduction of binding induced by introducing a Glu at

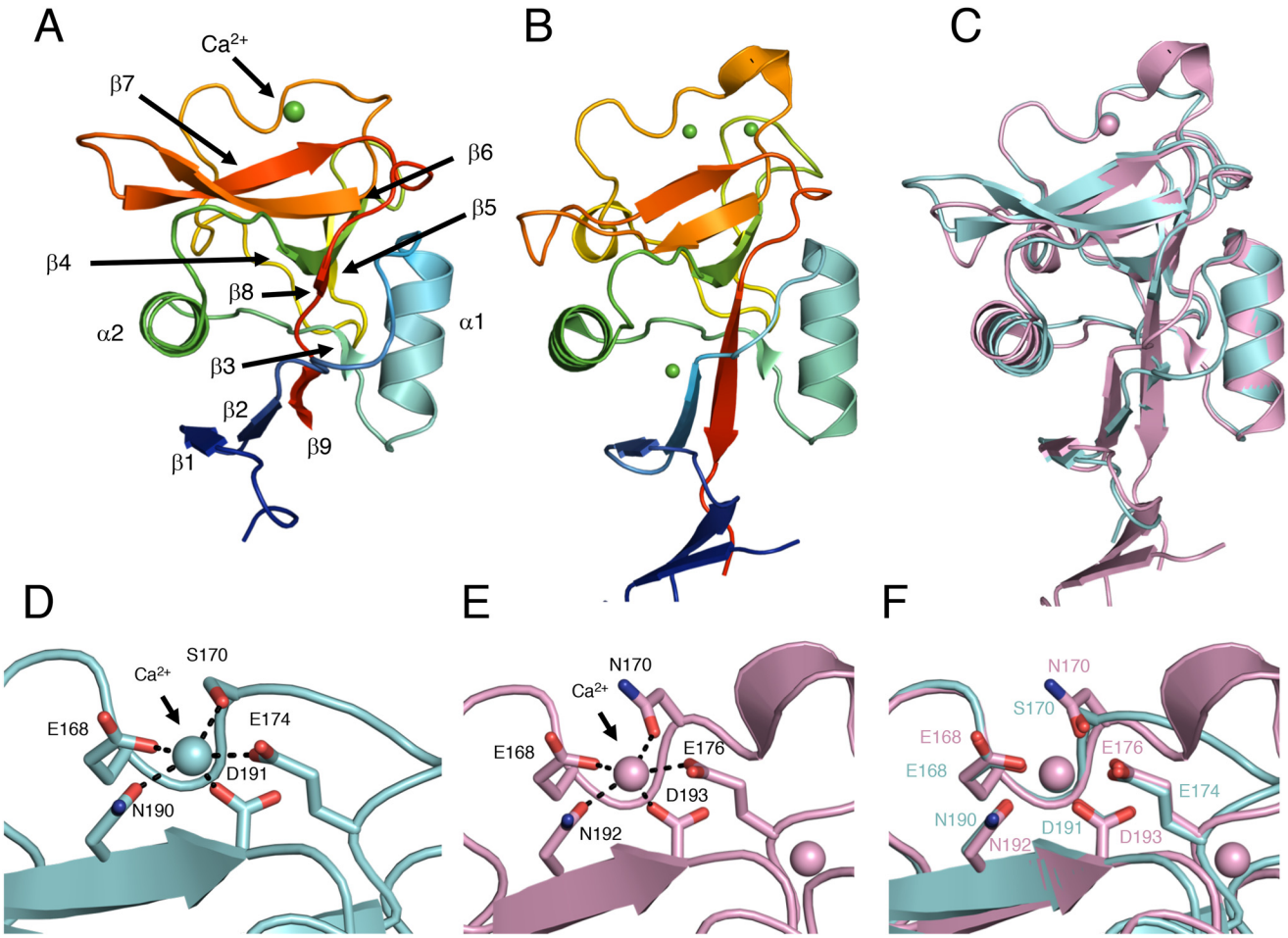

Figure 2. Comparison of the overall structure and Ca^{2+}-binding site of DCAR and Mincle. *A–C*, overall structures of DCAR (*A*, PDB code 6KZR) and cow Mincle (*B*, PDB code 4KZW). The *green spheres* indicate the position of Ca^{2+} ions in DCAR and Mincle. Residues from the N- to C-terminal end are shown by the *blue* to *red color gradient*. The superimposed structure of DCAR (*cyan*) and Mincle (*pink*) is shown in *C*. *D-F*, the primary sugar-binding sites of DCAR (*D*, *cyan*), Mincle (*E*, *pink*), and their superimposition (*F*) are shown in close-up view. The *spheres* represent Ca^{2+} ions and Ca^{2+} coordination bonds are depicted by *black dotted lines*. Oxygen and nitrogen atoms are shown in *red* and *blue*, respectively.

this position confirmed the detrimental effect of a negative charge near the primary sugar-binding site, as seen for Ala^{136} (Fig. S2*D*).

In hDCIR, hBDCA-2, and mDCIR2, an Asn corresponds to the Tyr^{180} of DCAR and interacts with the carbonyl group of the *N*-acetylglucosamine (GlcNAc) at the nonreducing end of mannose in all three structures (13, 15, 17, 18). Mutation of Tyr^{180} led to a partial reduction of reporter activity (Fig. S2*E*), suggesting that this residue is also involved in binding, but to a lesser extent than the Gln^{198}. Collectively, these results may therefore imply that DCAR binds an additional sugar of its ligands through a secondary sugar-binding site.

DCAR binds the phosphosaccharide moiety of AcPIMs

Among CLRs, DCAR has the uncommon characteristic of recognizing and binding phosphoglycolipids from mycobacteria such as AcPIM2 (Fig. 4*A*). We thus sought to investigate whether the sugar and phosphate moiety interacts with DCAR. We generated a soluble synthetic compound that comprises the phosphosaccharide moiety of AcPIM2 without lipid chains (inositol-monophosphate dimannose; IPM2), which can be used in aqueous binding assays (Fig. 4*A*, shaded in *blue*). We first attempted to inhibit binding of the DCAR–Ig fusion protein to plate-coated AcPIM2 by this analog (Fig. 4*A*). Contrary to free D-mannose, this compound induced a dose-dependent inhibition of DCAR–Ig binding to its ligand. These results suggest that DCAR has the potential to interact with at least mannose linked to inositol monophosphate.

To measure direct binding of DCAR–Ig to the analog IPM2, we turned to the sensitive biolayer interferometry (BLI) assay. Neither free mannose nor free D-*myo*-inositol (data not shown) could be bound by DCAR–Ig. Consistent with the competitive binding assay shown in Fig. 4*A*, real-time binding of DCAR–Ig, but not Ig, to the synthetic PIM analog was observed by BLI (Fig. 4*B*, *left panels*). In this experimental setting, steady-state analysis (Fig. 4*B*, *right panels*) demonstrated a dissociation constant (K_d) of 140 ± 7.9 μM. This result therefore indicated that within the whole ligand, DCAR has substantial affinity with the phosphosaccharide moiety.

DCAR complex structure with IPM2

We finally tried to verify this interaction by obtaining the structure of DCAR in complex with IPM2 (Fig. 5*A*). Co-crystals of the DCAR CRD–IPM2 complex were diffracted up to 1.84 Å

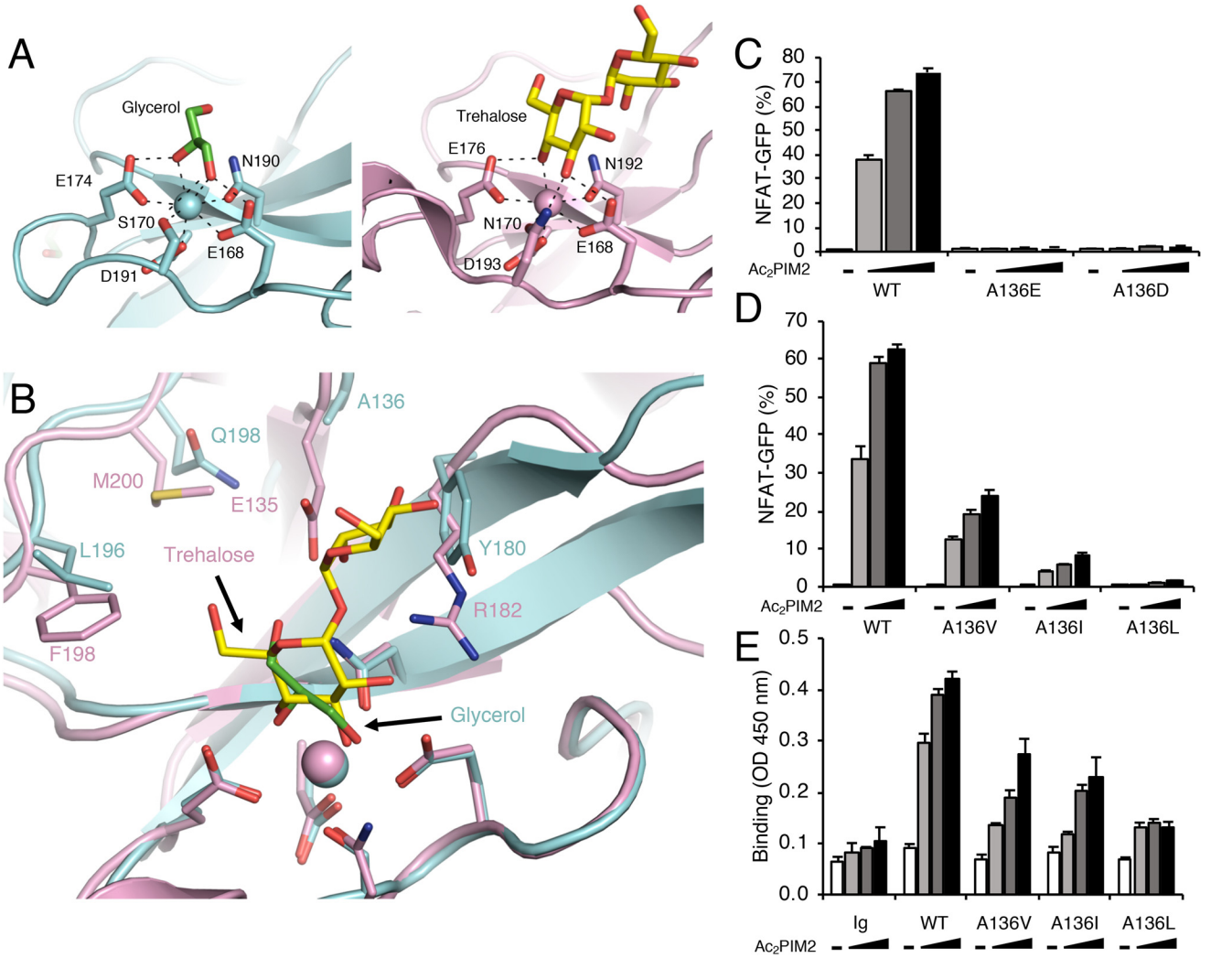

Figure 3. Structural comparison of the putative ligand-binding site of DCAR and Mincle. *A*, close-up view of the putative ligand-binding site of DCAR (*cyan*, *left panel*, PDB code 6KZR) and Mincle (*pink*, *right panel*, PDB code 4KZV) bound to glycerol (*green*) and trehalose (*yellow*), respectively. Hydrogen and Ca^{2+} coordination bonds are depicted by *black dotted lines*. *B*, superimposed structures of the residues adjacent to the putative binding site of glycerol-bound DCAR (*cyan*) and trehalose-bound Mincle (*pink*). *C* and *D*, reporter cells expressing DCAR or its mutants were stimulated with increasing amounts (30, 100, and 300 ng/well) of plate-coated Ac_2PIM2 for 18 h, and NFAT-GFP activity was assessed by flow cytometry. *E*, the Fc portion of human IgG (*Ig*), WT or mutant DCAR–Ig fusion proteins were incubated with increasing amounts (10, 30, and 100 ng/well) of plate-coated Ac_2PIM2, and binding was detected using anti-hIgG–horseradish peroxidase. The data are presented as the means ± S.D. of triplicate assays and are representative of three independent experiments (*C–E*).

resolution in the $P2_12_12_1$ space group, and two complexes were in the asymmetric unit. The electron density of IPM2 was clearly identified except for one mannose (Fig. 5*B*). The structure shows that DCAR interacts with mannose through the 3- and 4-OH groups (Fig. 5*A*), which confirms our assumption raised from the interaction with glycerol (Fig. 3*A*) and that DCAR binds mannose through its EPS motif. Importantly, we did not observe apparent conformational change upon ligand binding, which is often seen in "non-CLR" immune receptors (19, 20). Rather, ligand-free and IPM2-bound structures of DCAR were almost identical (Fig. 5, *C–E*), supporting the idea that CLRs do not utilize conformational changes as a strategy for signaling.

Contribution of a hydrophobic groove to the interaction with AcPIMs

Our analysis of DCAR binding to IPM2 by BLI showed that the interaction dissociated rapidly (Fig. 4*B*). This prompted us to determine whether another determinant may be involved in the interaction with the whole "acylated" ligands AcPIMs. The crystal structure revealed a hydrophobic area close to the IPM2-binding site (Fig. 6, *A* and *B*), which is in a suitable position to accommodate the acyl chains of AcPIMs. We therefore reduced the hydrophobicity of this area by substituting the Ile^{133} by Gly ($DCAR^{I133G}$) or Ala ($DCAR^{I133A}$). The DCAR reporter activity was strongly reduced for both mutants (Fig. 6*C*), whereas these mutations did not grossly disrupt the receptor structure and function (Fig. 6*D*). These results thus suggest that this hydrophobicity also contributes to the recognition of the mycobacterial AcPIMs via its receptor DCAR.

Discussion

We report here the atomic details of unique ligand recognition mode of the CRD of DCAR toward phosphoglycolipids. The Ca^{2+}-binding motifs of C-type lectins were shown to directly influence sugar specificity. Indeed, substituting the

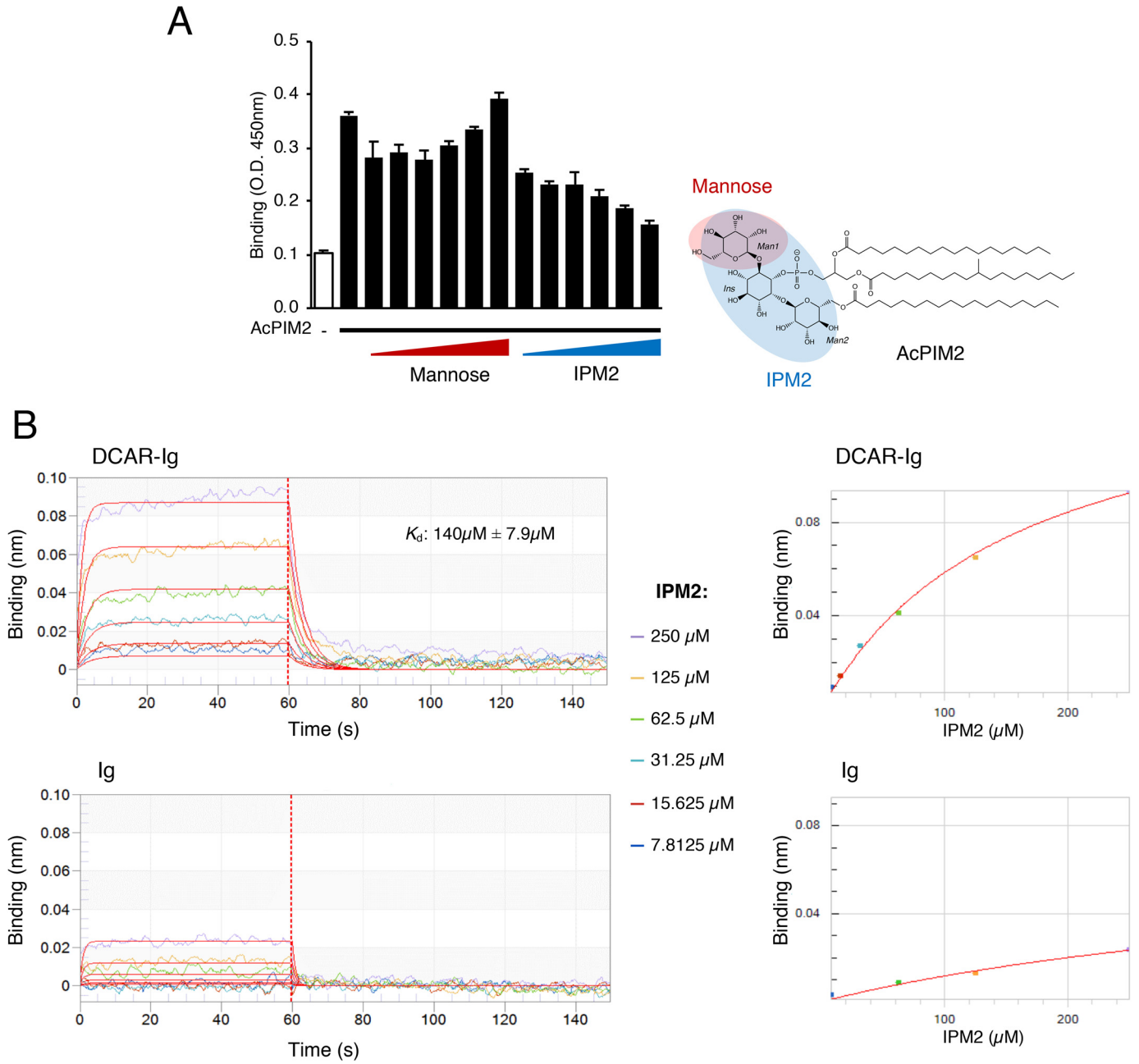

Figure 4. DCAR interacts with the AcPIM phosphosaccharide moiety. *A*, blocking of DCAR–Ig fusion protein binding to plate-coated AcPIM2 (150 ng/well) by increasing concentrations (0.0625, 0.125, 0.250, 0.5, 1, and 2 mM) of mannose and inositol-monophosphate dimannose (IPM2). The structure of both molecule is *shaded* in *red* and *blue*, respectively, on the structure of AcPIM2. Mannose and inositol residues are shown by *Man* and *Ins*, respectively. The data are presented as the means ± S.D. of triplicate assays and are representative of two independent experiments. *B*, analysis of the interaction between IPM2 and DCAR–Ig (*top panels*) or control Ig (*lower panels*) by biolayer interferometry. The fitting view is shown on the *left*, and the steady-state analysis is on the *right*.

EPN motif of rat MBP-A (mannose-binding protein A) by QPD imparts galactose binding ability to this C-type lectin (12). Although the EPN and EPS motifs both have previously been shown to bind mannose moieties (5, 13), here we show that having an EPN motif in lieu of EPS significantly reduces ligand recognition by DCAR. Interestingly, the amine group of Asn^{170} of $EPN_{168-170}$ makes a hydrogen bond with the 3-OH of glucose in the Mincle–trehalose complex (Fig. 3*A*, *right panel*), but the Ser^{170} in $EPS_{168-170}$ of DCAR does not have this hydrogen donor (Fig. 5*A* and Fig. S3*B*). It may therefore be plausible that the EPS motif sets the ligand in a different position than the EPN, which could contribute to efficient ligand binding by DCAR. Thus, the C-type lectins may have evolved to recognize a broader spectrum of ligands by mutational changes in their binding motifs while retaining their overall canonical fold. Indeed, several unconventional EPN-like motifs, such as EPS and EPK, are found in C-type lectins across species (5, 10, 21, 22).

DCAR belongs to the DCIR family of CLRs, which share structural and ligand-binding similarities. Among them, the secondary binding site of hBDCA-2 and mDCIR2 interacts with GlcNAc linked to mannose (13, 15, 17). The Asn^{184} and Arg^{186} of hBDCA-2 interact with the carbonyl group of GlcNAc. Although the Arg (residue 182) is conserved in DCAR, the res-

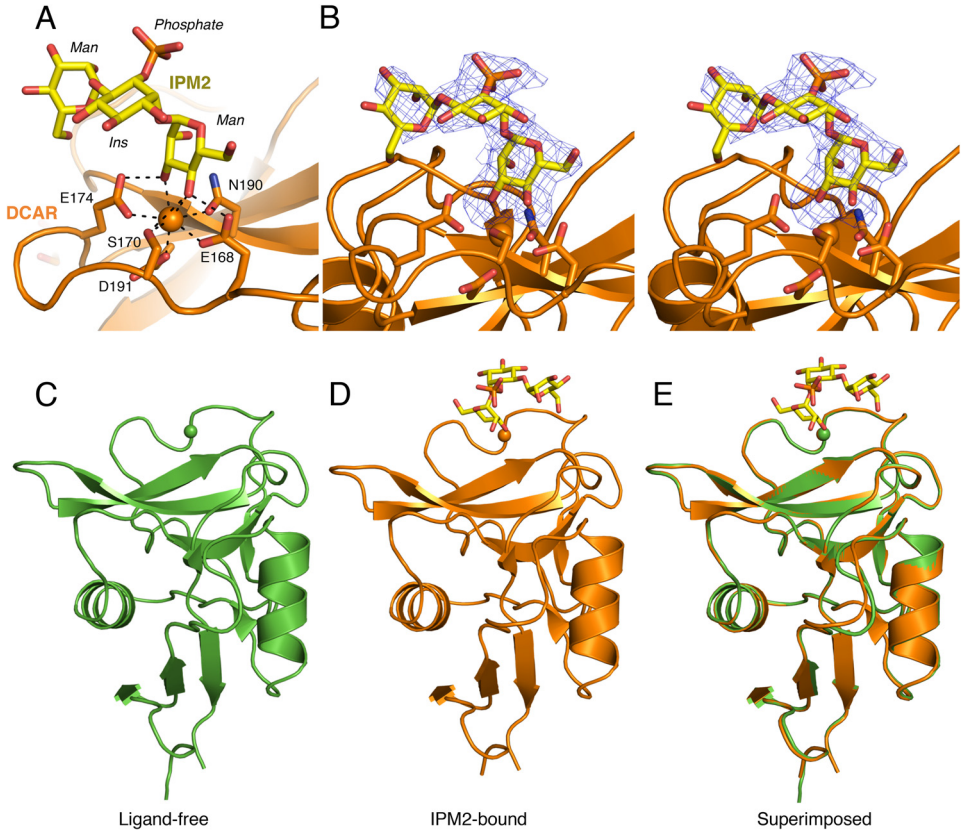

Figure 5. Crystal structure of the DCAR CRD in complex with IPM2. *A*, close-up view of the ligand-binding site bound to IPM2 (PDB code 6LFJ). Hydrogen and Ca^{2+} coordination bonds are depicted by *black dotted lines*, and IPM2 is in *yellow*. Mannose and inositol residues are shown by *Man* and *Ins*, respectively. *B*, stereo view of the omit map contoured at 1.9 σ level around IPM2 and shown by a *blue mesh*. *C–E*, overall structure of the ligand-free DCAR CRD (ligand-free, PDB code 6LKR) (*C*), the IPM2 complex (IPM2-bound) (*D*), and their superimposition (superimposed; root-mean-square deviation of 0.117 Å for 264 structurally equivalent Cα atoms) (*E*). The *spheres* represent Ca^{2+} ions.

idue corresponding to the Asn of hBDCA-2 is Tyr^{180}. Therefore, the hydrogen bond network with GlcNAc seen in hBDCA-2 would not be feasible for DCAR. mDCIR2 also binds GlcNAc through two additional residues (Asp^{223} and His^{225}), but they are not conserved in DCAR. This shows that although DCAR shares structural similarities with DCIR family members, it possesses fine characteristic structural features to achieve its unique specificity.

The loop region between the β2 and β3 strands of mDCIR2 was suggested to create a narrow carbohydrate-binding site when compared with dendritic cell–specific ICAM-3 grabbing nonintegrin (DC-SIGN), which would lead to lower affinity for high mannose ligands. It was also proposed that this may be a conserved feature among DCIR family members (15). Interestingly, we have previously shown that among the AcPIM species, which vary in their number of mannose residues, DCAR activation and binding weakens as the number of mannose increases (Fig. S4*A*), whereas the opposite tendency was observed for DC-SIGN (Fig. S4*B*) (7). Because the β6-β7 loop of DCAR also generates a narrow binding site when compared with that of DC-SIGN (Fig. S4*C*), it could explain DCAR poor binding to AcPIM6 and Ac_2PIM6. Our data therefore corroborate this hypothesis, and the characteristic narrow carbohydrate-binding site may indeed be shared by DCIR family CLRs, which may contribute to their specificity for low mannose ligands.

Our complex analysis clearly demonstrated the interaction of mannose to DCAR. Although inositol and phosphate were not observed in the proximity of the CRD from the co-crystal structure with IPM2, it does not exclude the possible contribution of phosphate and inositol in the context of whole AcPIMs. Indeed, our BLI analysis suggests that DCAR can interact with the phosphosaccharide IPM2 but not with mannose alone. Similarly, IPM2, but not monosaccharide, was able to block the interaction between DCAR and AcPIM2 (Fig. 4*A*).

However, the interaction of DCAR CRD and IPM2 was transient and dissociated rapidly, implying that another additional determinant also contributes to stable interaction, which may be required for optimal signal transduction through DCAR. Mincle was shown to have a hydrophobic region close to the primary sugar-binding site that allows the accommodation of the lipid moiety of its ligands (11, 23). The structure of DCAR also shows a hydrophobic surface, although in a different area than that of Mincle, extending from the primary sugar-binding site (Fig. 6, *A* and *B*), which also contributed to the AcPIM binding (Fig. 6*C*).

Acylated PIMs may have up to four acyl chains; there are two within the phosphatidyl moiety, and for AcPIM2, one additional chain is linked to the 6-OH of the Man2 residue (Fig. 4*A*). Based on the DCAR–IPM2 complex, one mannose residue is bound at the primary sugar-binding site, and its 6-OH would be in a suitable position to allow an acyl chain to interact with the

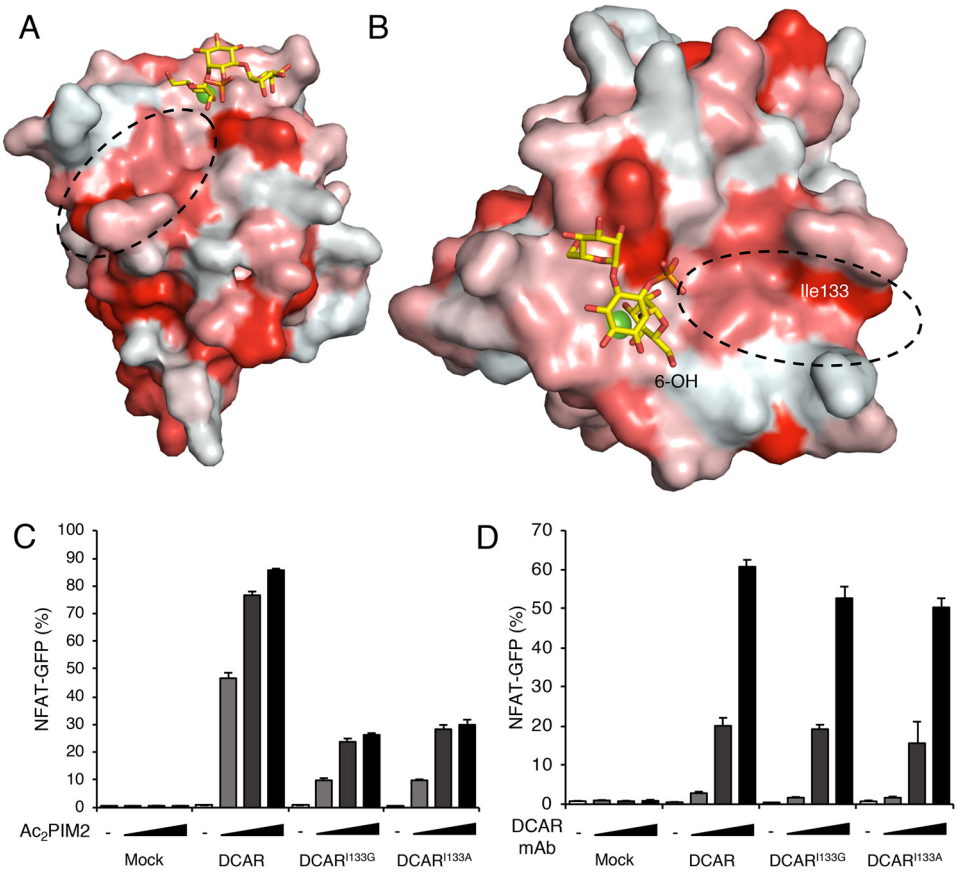

Figure 6. Contribution of a hydrophobic groove to binding with AcPIMs. *A* and *B*, overall (*A*) and close-up view of the primary sugar-binding site (*B*). Hydrophobicity is represented by a *white* (hydrophilic) to *red* (hydrophobic) gradient. The *dotted oval* shows the possible acyl chain–binding site, and the positions of the Ile^{133} and 6-OH of the bound mannose are shown in *white* and *black*, respectively. The *green sphere* indicates the position of the Ca^{2+} ion. *C* and *D*, reporter cells expressing FcRγ only (*Mock*) or together with DCAR, $DCAR^{I133G}$, or $DCAR^{I133A}$ were stimulated with increasing amounts (30, 100, and 300 ng/well) of plate-coated Ac_2PIM2 (*C*) or by coated anti-DCAR mAb (*D*). The data are presented as the means ± S.D. of triplicate assays and are representative of two independent experiments.

hydrophobic groove (Fig. 6*B*). Additionally, the position of the phosphate group of IPM2 suggests that the phosphatidyl moiety may also be bound by the hydrophobic area, which could bring the phosphate and inositol within interacting distance of Ala^{136}, Tyr^{180}, and Gln^{198}. This may explain the strong reduction of ligand binding by mutation of these residues observed in response to whole AcPIMs. Thus, these two lectins for mycobacteria may have independently acquired the structural feature conferring the ability to recognize not only sugars but also lipids, because the primary structure corresponding to the putative hydrophobic grooves were different between Mincle and DCAR.

Signaling through C-type lectin receptors requires their multimerization by the recognition of multivalent ligands, thereby inducing the phosphorylation of ITAM within their signaling subunits (24, 25). Therefore, theoretically these receptors do not necessarily require ligand-induced conformational change, which is usually a critical process for other receptors, such as cytokine receptors or G protein–coupled receptors. Indeed, we did not observe any drastic conformational changes of DCAR CRD after IPM2 binding (Fig. 5, *C* and *D*). Thus, although DCAR is able to recognize one ligand molecule, AcPIMs can signal through DCAR only when it is presented on the bacteria at high valency. This may be an additional strategy to discriminate real pathogens from the presence of structurally similar glycolipids that should not trigger immune responses in the host. Indeed, IPM2 did not activate cells expressing DCAR (data not shown), although it bound to DCAR (Fig. 4*B*).

The structural analysis of DCAR revealed particular features allowing this receptor to bind phosphate-containing ligands, implying the presence of other pathogen- or host-derived phosphoglycolipids recognized by this CLR. Because no homolog of DCAR was found in the human Dectin-2 cluster, the structure of mouse DCAR may contribute to a rational structural approach toward the identification of a functional homolog or unknown receptor(s) for AcPIMs in human.

Experimental procedures

Reagents

AcPIM2 and Ac_2PIM2 were purified from mycobacterial crude lipids as described previously (7). Anti-mouse DCAR rat mAb (MAB2757, clone 349214) was purchased from R&D Systems.

Recombinant protein expression and purification

The CRD of mouse DCAR (residues C78-L209) was inserted in the *E. coli* expression plasmid pGMT7 (primers are shown in Table S1), which then was transformed into the *E. coli* strain

Rosetta™ (DE3) (Novagen). Because of a cloning artifact, three additional amino acids were expressed at the N-terminal end upstream of the C78. Transformants were grown in selective LB medium, protein expression was induced with 0.5 mM isopropyl β-D-thiogalactoside (Nacalai Tesque Inc.), and the cells were cultured for 3 h. The cells were then harvested at 4000 rpm for 20 min, resuspended in lysis buffer (10 mM Tris-HCl, pH 8.0, 10 mM $MgCl_2$, 150 mM NaCl, 10% glycerol) and disrupted by sonication. After a 30-min DNase I (Roche, 100 μg/ml) treatment, inclusion bodies were purified by centrifugation. Inclusion bodies were solubilized in a buffer containing 6 M guanidine, 50 mM Tris-HCl, pH 8.0, 100 mM NaCl, 2 mM EDTA. DTT (10 mM) was then added to solubilized proteins, which were then slowly incorporated into a refolding buffer containing 100 mM Tris-HCl, pH 8.0, 2 mM EDTA, 0.4 M L-arginine, 6.5 mM cysteamine, 3.6 mM cystamine and slowly stirred at 4 °C for at least 3 h. The proteins were then dialyzed twice against 10 mM Tris-HCl, pH 8.0, and purified by anion exchange (Poros® 50 HQ column, Applied Biosystems) and size-exclusion (Superdex™ 200 10/300 column, GE healthcare) chromatography. The fractions corresponding to the DCAR CRD were pooled and enriched using an Amicon Ultra centrifugal filter (molecular weight cut-off: 3000, Merck Millipore) for crystallization assays.

Crystallization and structure determination

All crystals were generated by crystallizing purified recombinant DCAR (10 mg/ml for ligand-free and DCAR–IPM2 complex and 13 mg/ml for DCAR– glycerol complex) using the sitting-drop vapor-diffusion method at 20 °C. DCAR– glycerol complex crystals were obtained by growing crystals for 4 days under a reservoir solution consisting of 0.04 M citric acid, 0.06 M Bis-Tris propane, pH 6.4, 20% (w/v) PEG 3350, 10 mM $CaCl_2$. For data collection, the crystals were transferred to the cryo buffer (0.04 M citric acid, 0.06 M Bis-Tris propane, pH 6.4, 22% (w/v) PEG 3350, 10 mM $CaCl_2$, 15% glycerol). Ligand-free and DCAR–IPM2 complex crystals were grown for 7 days under a reservoir solution consisting of 0.04 M citric acid, 0.06 M Bis-Tris propane, pH 6.4, 35% (w/v) PEG 3350, 10 mM $CaCl_2$, with or without 120 mM IPM2. For data collection, the crystals were frozen directly from the drop in liquid nitrogen. Thereafter, all crystals were flash-frozen using a cryo system (Rigaku). X-ray diffraction data sets were collected on Beamline BL45XU at SPring-8 (Hyogo, Japan). The diffraction data were processed using the program package XDS (26). The crystals were found to belong to space group $P2_12_12_1$. The data collection statistics are compiled in Table 1. The crystal structure of the DCAR– glycerol complex was determined by molecular replacement using Molrep (27) with the template structure (PDB code 3VYJ), and the ligand-free and IPM2-complex structures were obtained by molecular replacement using the glycerol-complex structure. The structures were manually modified using the Coot program (28). Several iterative rounds of model building were performed in Coot and refined using Refmac5 (29). Refinement statistics are summarized in Table 1. The quality of the structures was assessed using PROCHECK (30).

Synthesis of IPM2

The IPM2 analog having D-*myo*-inositol 1-phosphate was chemically synthesized from D-mannose and commercially available D-glucose derivative. First, D-*myo*-inositol acceptor was prepared from methyl α-D-glucopyranoside via 10 reaction steps according to the literature (31). Moffat oxidation of the primary alcohol of 2,3,4-tri-*O*-benzyl-protected glucoside, which was derived from methyl α-D-glucopyranoside via three steps, followed by treatment with acetic anhydride provided the *Z*-olefin product in good yields. Subsequent treatment of the olefin with palladium chloride afforded the 3-OH penta-oxygenated cyclohexanone derivative. The reduction of the resulting cyclic ketone with $Me_4NBH(OAc)_3$ provided the diol derivative of D-*myo*-inositol, which was then converted into the inositol diol acceptor with the allyl group at the C-1 position via three steps. On the other hand, 2-*O*-acetyl-3,4,6-tri-*O*-benzyl-α-D-mannopyranosyl trichloroacetimidate donor to be coupled with the inositol acceptor was readily prepared from D-mannose via seven steps. The glycosylation of the inositol acceptor with the mannose donor was performed in the presence of trimethyl trifluoromethanesulfonate in diethyl ether at 0 °C, affording the dimannoside in good yield and α-selectivity. Removal of the allyl group was then conducted by treatment of the dimannoside with Ir complex under hydrogen atmosphere in THF followed by hydrolysis with aqueous HCl, giving the alcohol in 93% yield. The phosphoester linkage was introduced to the C-1 position of the inositol residue by coupling with dibenzyl *N*,*N*-diisopropylphosphoramidite and 1*H*-tetrazole in CH_2Cl_2 and subsequent *m*-CPBA oxidation, affording the fully protected IPM2 analog in 84% yield. The final steps involved deacetylation and hydrogenolytic debenzylation to furnish the target IPM2 analog in good yields. The structure of IPM2 was verified by NMR and MS (Fig. S5–S8).

Binding assay

Mouse DCAR–Ig fusion proteins (WT and mutants) were generated as previously described (32). In brief, the extracellular domain of DCAR (residues 42–209) was fused to the N-terminal end of the hIgG1 Fc region. Fusion proteins were then incubated with increasing amounts of plate-coated AcPIMs (10, 30, and 100 ng/well), and bound proteins were detected using horseradish peroxidase–labeled anti-human IgG (Jackson ImmunoResearch). After the addition of the colorimetric substrate, peroxidase activity was measured using a spectrophotometer. The mutant Ig fusion proteins were generated by recombinant PCR (primers are shown in Table S1).

Reporter assay

2B4-NFAT-GFP reporter cells were prepared as previously described (32). Briefly, we induced stable expression of FcRγ and DCAR or its mutants (generated by recombinant PCR; primers are shown in Table S1), and the cells were stimulated with increasing amounts of plate-coated AcPIMs (30, 100 and 300 ng/well) or anti-mouse DCAR rat mAb (MAB2757, clone 349214, R&D Systems; 0.3, 1, and 3 μg/ml). GFP expression was then assessed by flow cytometry.

Biolayer interferometry

The Octet RED96 System (fortéBio, Pall Life Science) was used to measure the binding kinetics of DCAR–Ig fusion proteins to the synthetic AcPIM phosphosaccharide moiety, IPM2. The binding is measured by the shift of wavelength caused by the interaction between the two molecules on the surface of the biosensor. All assays were carried out at 25 °C on a black 96-well plate (Greiner, Bio-One), with agitation set at 1000 rpm and 200 μl/well for each solution. Super streptavidin biosensors (fortéBio, Pall Life Science) were prewetted in TSM buffer (20 mM Tris-HCl, pH 7.0, 150 mM NaCl, 1 mM $CaCl_2$, 2 mM $MgCl_2$) for 10 min. The CaptureSelect™ Biotin anti-IgG–Fc conjugate (Thermo Fisher) was then loaded onto the biosensors to saturation (2 μg/ml in TSM buffer). Capture of the DCAR–Ig fusion protein (100 μg/ml in TSM buffer) was performed to saturation as well. Association to IPM2 was followed for 60 s and dissociation for 90 s. 2-fold concentration gradient of the compound was used in a titration series of six. Baseline drift was corrected by subtracting the shift of a sensor loaded with fusion protein but incubated in buffer only. Nonspecific binding was assessed by performing the assay with the Fc portion of human IgG (Ig). Octet data were analyzed and processed using the Octet data analysis 11.1 software.

Author contributions—Z. O. and S. Y. conceptualization; S. Y. supervision; Z. O., Y. H., M. N., K. Toyonaga, and A. I. investigation; Z. O., Y. H., M. N., K. Toyonaga, and S. Y. writing-original draft; Z. O., Y. H., M. N., K. Toyonaga, A. I., K. Takato, Y. K., and S. Y. writing-review and editing; A. I., K. Takato, T. T., and H. I. resources; T. T. and Y. K. data curation; Y. H., T. T., and Y. K. crystallographic experiments.

Acknowledgments—We thank C. Motozono, T. Shimamura, T. Seguchi, F. Sugihara, the staff of the Central instrumentation laboratory of the Research Institute for Microbial Diseases, Osaka University, and the Cooperative Research Project Program of the Medical Institute of Bioregulation, Kyushu University for technical assistance and discussion. We thank the staff members of SPring-8 for help with data collection. This research was undertaken in part using Beamline BL45XU at SPring-8, Hyogo, Japan.

References

1. Akira, S., Uematsu, S., and Takeuchi, O. (2006) Pathogen recognition and innate immunity. *Cell* **124,** 783–801 CrossRef Medline
2. Hoving, J. C., Wilson, G. J., and Brown, G. D. (2014) Signalling C-type lectin receptors, microbial recognition and immunity. *Cell Microbiol.* **16,** 185–194 CrossRef Medline
3. Sancho, D., Joffre, O. P., Keller, A. M., Rogers, N. C., Martínez, D., Hernanz-Falcón, P., Rosewell, I., and Reis e Sousa, C. (2009) Identification of a dendritic cell receptor that couples sensing of necrosis to immunity. *Nature* **458,** 899–903 CrossRef Medline
4. Nagata, M., Izumi, Y., Ishikawa, E., Kiyotake, R., Doi, R., Iwai, S., Omahdi, Z., Yamaji, T., Miyamoto, T., Bamba, T., and Yamasaki, S. (2017) Intracellular metabolite β-glucosylceramide is an endogenous Mincle ligand possessing immunostimulatory activity. *Proc. Natl. Acad. Sci. U.S.A.* **114,** E3285–E3294 CrossRef Medline
5. Zelensky, A. N., and Gready, J. E. (2005) The C-type lectin-like domain superfamily. *FEBS J.* **272,** 6179–6217 CrossRef Medline
6. Kanazawa, N., Tashiro, K., Inaba, K., and Miyachi, Y. (2003) Dendritic cell immunoactivating receptor, a novel C-type lectin immunoreceptor, acts as an activating receptor through association with Fc receptor γ chain. *J. Biol. Chem.* **278,** 32645–32652 CrossRef Medline
7. Toyonaga, K., Torigoe, S., Motomura, Y., Kamichi, T., Hayashi, J. M., Morita, Y. S., Noguchi, N., Chuma, Y., Kiyohara, H., Matsuo, K., Tanaka, H., Nakagawa, Y., Sakuma, T., Ohmuraya, M., Yamamoto, T., *et al.* (2016) C-type lectin receptor DCAR recognizes mycobacterial phosphatidyl-inositol mannosides to promote a Th1 response during infection. *Immunity* **45,** 1245–1257 CrossRef Medline
8. Guerin, M. E., Korduláková, J., Alzari, P. M., Brennan, P. J., and Jackson, M. (2010) Molecular basis of phosphatidyl-myo-inositol mannoside biosynthesis and regulation in mycobacteria. *J. Biol. Chem.* **285,** 33577–33583 CrossRef Medline
9. Kerscher, B., Willment, J. A., and Brown, G. D. (2013) The Dectin-2 family of C-type lectin-like receptors: an update. *Int. Immunol.* **25,** 271–277 CrossRef Medline
10. Flornes, L. M., Bryceson, Y. T., Spurkland, A., Lorentzen, J. C., Dissen, E., and Fossum, S. (2004) Identification of lectin-like receptors expressed by antigen presenting cells and neutrophils and their mapping to a novel gene complex. *Immunogenetics* **56,** 506–517 CrossRef Medline
11. Feinberg, H., Jégouzo, S. A., Rowntree, T. J., Guan, Y., Brash, M. A., Taylor, M. E., Weis, W. I., and Drickamer, K. (2013) Mechanism for recognition of an unusual mycobacterial glycolipid by the macrophage receptor Mincle. *J. Biol. Chem.* **288,** 28457–28465 CrossRef Medline
12. Drickamer, K. (1992) Engineering galactose-binding activity into a C-type mannose-binding protein. *Nature* **360,** 183–186 CrossRef Medline
13. Nagae, M., Ikeda, A., Hanashima, S., Kojima, T., Matsumoto, N., Yamamoto, K., and Yamaguchi, Y. (2016) Crystal structure of human dendritic cell inhibitory receptor C-type lectin domain reveals the binding mode with *N*-glycan. *FEBS Lett.* **590,** 1552 CrossRef Medline
14. Feinberg, H., Rambaruth, N. D., Jégouzo, S. A., Jacobsen, K. M., Djurhuus, R., Poulsen, T. B., Weis, W. I., Taylor, M. E., and Drickamer, K. (2016) Binding sites for acylated trehalose analogs of glycolipid ligands on an extended carbohydrate recognition domain of the macrophage receptor Mincle. *J. Biol. Chem.* **291,** 21222–21233 CrossRef Medline
15. Nagae, M., Yamanaka, K., Hanashima, S., Ikeda, A., Morita-Matsumoto, K., Satoh, T., Matsumoto, N., Yamamoto, K., and Yamaguchi, Y. (2013) Recognition of bisecting N-acetylglucosamine: structural basis for asymmetric interaction with the mouse lectin dendritic cell inhibitory receptor 2. *J. Biol. Chem.* **288,** 33598–33610 CrossRef Medline
16. Feinberg, H., Jégouzo, S. A. F., Rex, M. J., Drickamer, K., Weis, W. I., and Taylor, M. E. (2017) Mechanism of pathogen recognition by human dectin-2. *J. Biol. Chem.* **292,** 13402–13414 CrossRef Medline
17. Jégouzo, S. A., Feinberg, H., Dungarwalla, T., Drickamer, K., Weis, W. I., and Taylor, M. E. (2015) A novel mechanism for binding of galactose-terminated glycans by the C-type carbohydrate recognition domain in blood dendritic cell antigen 2. *J. Biol. Chem.* **290,** 16759–16771 CrossRef Medline
18. Nagae, M., Ikeda, A., Kitago, Y., Matsumoto, N., Yamamoto, K., and Yamaguchi, Y. (2014) Crystal structures of carbohydrate recognition domain of blood dendritic cell antigen-2 (BDCA2) reveal a common domain-swapped dimer. *Proteins* **82,** 1512–1518 CrossRef Medline
19. Liongue, C., Sertori, R., and Ward, A. C. (2016) Evolution of cytokine receptor signaling. *J. Immunol.* **197,** 11–18 CrossRef Medline
20. Pelka, K., Shibata, T., Miyake, K., and Latz, E. (2016) Nucleic acid-sensing TLRs and autoimmunity: novel insights from structural and cell biology. *Immunol. Rev.* **269,** 60–75 CrossRef Medline
21. Haurum, J. S., Thiel, S., Haagsman, H. P., Laursen, S. B., Larsen, B., and Jensenius, J. C. (1993) Studies on the carbohydrate-binding characteristics of human pulmonary surfactant-associated protein A and comparison with two other collectins: mannan-binding protein and conglutinin. *Biochem. J.* **293,** 873–878 CrossRef Medline
22. Poget, S. F., Legge, G. B., Proctor, M. R., Butler, P. J., Bycroft, M., and Williams, R. L. (1999) The structure of a tunicate C-type lectin from *Polyandrocarpa misakiensis* complexed with D-galactose. *J. Mol. Biol.* **290,** 867–879 CrossRef Medline
23. Furukawa, A., Kamishikiryo, J., Mori, D., Toyonaga, K., Okabe, Y., Toji, A., Kanda, R., Miyake, Y., Ose, T., Yamasaki, S., and Maenaka, K. (2013) Structural analysis for glycolipid recognition by the C-type lectins Mincle and MCL. *Proc. Natl. Acad. Sci. U.S.A.* **110,** 17438–17443 CrossRef Medline

24. Goodridge, H. S., Reyes, C. N., Becker, C. A., Katsumoto, T. R., Ma, J., Wolf, A. J., Bose, N., Chan, A. S., Magee, A. S., Danielson, M. E., Weiss, A., Vasilakos, J. P., and Underhill, D. M. (2011) Activation of the innate immune receptor Dectin-1 upon formation of a "phagocytic synapse." *Nature* **472,** 471–475 Medline
25. Iborra, S., and Sancho, D. (2015) Signalling versatility following self and non-self sensing by myeloid C-type lectin receptors. *Immunobiology* **220,** 175–184 CrossRef Medline
26. Kabsch, W. (2010) XDS. *Acta Crystallogr. D Biol. Crystallogr.* **66,** 125–132 CrossRef Medline
27. Vagin, A., and Teplyakov, A. (2000) An approach to multi-copy search in molecular replacement. *Acta Crystallogr. D Biol. Crystallogr.* **56,** 1622–1624 CrossRef Medline
28. Emsley, P., and Cowtan, K. (2004) Coot: model-building tools for molecular graphics. *Acta Crystallogr. D Biol. Crystallogr.* **60,** 2126–2132 CrossRef Medline
29. Murshudov, G. N., Vagin, A. A., and Dodson, E. J. (1997) Refinement of macromolecular structures by the maximum-likelihood method. *Acta Crystallogr. D Biol. Crystallogr.* **53,** 240–255 CrossRef Medline
30. Vaguine, A. A., Richelle, J., and Wodak, S. J. (1999) SFCHECK: a unified set of procedures for evaluating the quality of macromolecular structure–factor data and their agreement with the atomic model. *Acta Crystallogr. D Biol. Crystallogr.* **55,** 191–205 CrossRef Medline
31. Takahashi, H., Kittaka, H., and Ikegami, S. (2001) Novel synthesis of enantiomerically pure natural inositols and their diastereoisomers. *J. Org. Chem.* **66,** 2705–2716 CrossRef Medline
32. Yamasaki, S., Ishikawa, E., Sakuma, M., Hara, H., Ogata, K., and Saito, T. (2008) Mincle is an ITAM-coupled activating receptor that senses damaged cells. *Nat. Immunol.* **9,** 1179–1188 CrossRef Medline
33. Gouet, P., Robert, X., and Courcelle, E. (2003) ESPript/ENDscript: extracting and rendering sequence and 3D information from atomic structures of proteins. *Nucleic Acids Res.* **31,** 3320–3323 CrossRef Medline